

A flexible strain gauge exhibiting reversible piezoresistivity based on an anisotropic magnetorheological polymer

This content has been downloaded from IOPscience. Please scroll down to see the full text.

2014 Smart Mater. Struct. 23 085026

(<http://iopscience.iop.org/0964-1726/23/8/085026>)

View [the table of contents for this issue](#), or go to the [journal homepage](#) for more

Download details:

IP Address: 200.0.233.52

This content was downloaded on 19/02/2015 at 18:06

Please note that [terms and conditions apply](#).

A flexible strain gauge exhibiting reversible piezoresistivity based on an anisotropic magnetorheological polymer

José L Mietta¹, Guillermo Jorge^{2,3} and R Martín Negri¹

¹Instituto de Química Física de Materiales, Ambiente y Energía (INQUIMAE). Departamento de Química Inorgánica, Analítica y Química Física, Facultad de Ciencias Exactas y Naturales, Universidad de Buenos Aires, Argentina

²Instituto de Ciencias, Universidad Nacional de General Sarmiento, Argentina

E-mail: rmn@qi.fcen.uba.ar


Received 14 March 2014, revised 10 May 2014

Accepted for publication 16 May 2014

Published 2 July 2014

Abstract

A flexible, anisotropic and portable stress sensor (logarithmic reversible response between 40–350 kPa) was fabricated, in which i) the sensing material, ii) the electrical contacts and iii) the encapsulating material, were based on polydimethylsiloxane (PDMS) composites. The sensing material is a slide of an anisotropic magnetorheological elastomer (MRE), formed by dispersing silver-covered magnetite particles ($\text{Fe}_3\text{O}_4@\text{Ag}$) in PDMS and by curing in the presence of a uniform magnetic field. Thus, the MRE is a structure of electrically conducting pseudo-chains (*needles*) aligned in a specific direction, in which electrical conductivity increases when stress is exclusively applied in the direction of the needles. Electrical conductivity appears only between contact points that face each other at both sides of the MRE slide. An array of electrical contacts was implemented based on PDMS-silver paint metallic composites. The array was encapsulated with PDMS. Using Fe_3O_4 superparamagnetic nanoparticles also opens up possibilities for a magnetic field sensor, due to the magnetoresistance effects.

 Online supplementary data available from stacks.iop.org/SMS/23/085026/mmedia

Keywords: structured magnetoelastomer composites, piezoresistivity, flexible stress sensor, electrically conductive composite

(Some figures may appear in colour only in the online journal)

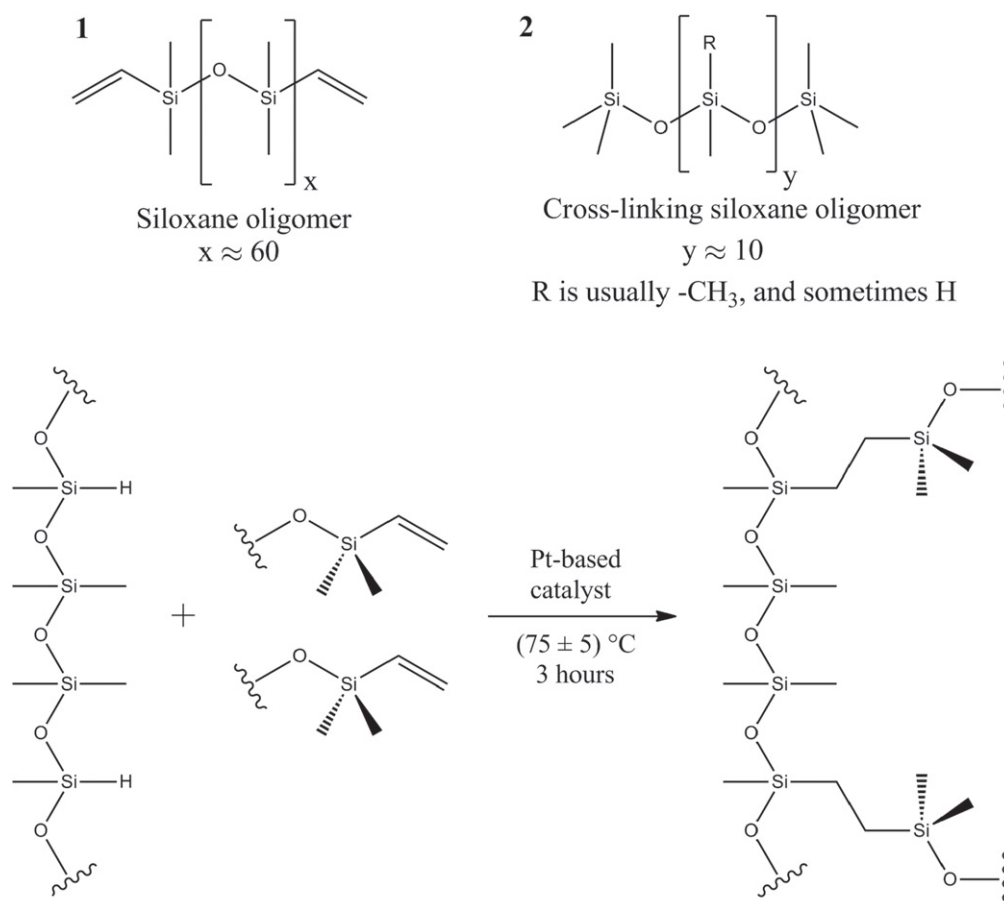
1. Introduction

Magnetorheological (MR) materials are materials with mechanical properties that can be modified by externally applied magnetic fields. One type of MR material is made of composites that are formed by dispersing magnetic filler particles into an elastomer polymeric matrix and then orientating the particles. These materials, referred to as magnetorheological elastomers (MRE), are promising for the application and development of polymer-based

electronic devices [1]. A simple procedure used to obtain MRE involves curing the filler-elastomer composite in the presence of a uniform magnetic field ($\mathbf{H}_{\text{curing}}$), which induces agglomerations of the filler particles into chain-like structures aligned in the direction of the $\mathbf{H}_{\text{curing}}$ [2–6]. In spite of their potential applications, there are two closely related aspects concerning MRE that have not been systematically explored yet: 1) the dependence of other physical properties (different than elasticity) with external driving forces, and 2) the implementation of real devices based on MRE, which is still in the preliminary phase [7–12].

In previous works done by our group, anisotropic MRE, using silver-covered Fe_3O_4 microparticles as fillers in

³ On leave from Laboratorio de Bajas Temperaturas, Universidad de Buenos Aires, Argentina.



Scheme 1. Scheme of the formation of a cross-linked network through hydrosilylation reaction in PDMS materials.

polydimethylsiloxane (PDMS) matrixes, were characterized and used for the implementation of 2D elastic Zebra®-like electrical connectors [13–15]. Elasticity changes under an applied magnetic field was observed in similar systems; however, Ni nanotubes and nanoparticles were used [16]. In the present work, the fabrication and characterization of a flexible and portable stress sensor array, based on the MRE, is shown. The array has excellent sensitivity and a reversible electrical response to external mechanical forces. The system is very robust against the action of various chemical agents (such as organic solvents), and its response has a very low variation, with temperatures in the range 25–155 °C.

Furthermore, use of a hybrid superparamagnetic inorganic filler in the magnetorheological material described in the present work constitutes a significant improvement compared to the fillers used in previously reported materials [17–19] since, using a superparamagnetic filler, the sensor array system has the essential feature of not being irreversibly magnetized at room temperature. The superparamagnetic behavior at room temperature provides a relatively fast magnetic relaxation also (loss of magnetization after canceling the applied external magnetic field occurs faster than the time resolution of our setup, 3 s). These features, along with the

decrease in electrical resistance by application of a magnetic field (negative magnetoresistance), open up the possibility of implementing the described sensor as a magnetic field sensor.

Physicochemical characterization of the MRE material (the active sensing material) that is involved in the sensor and that constitutes the basis of its performance, has already been described in previous works [13, 14, 20, 21]. Hence, the present paper describes the implementation of a chemically resistant, flexible, anisotropic and portable sensor. Relevant technological difficulties were overcome, such as the manufacture of electrical contacts on the surface of a magnetorheological polymer and the building-up of an array with reproducible behavior.

The *sensor* is constituted by two central components: 1) the active sensing material (referred to as MRE material) and 2) the electrical contacts (referred as PDMS-Ag paint contacts). Therefore, three concepts are distinguished through the article: 1) the *MRE material*, 2) the *electrical contacts* and 3) the fully packaged terminated *sensor*. In addition, the implementation of several contacts on the top and bottom surface of the MRE material allowed us to obtain an *array* of sensors, since the sensors are non-electrically connected because of the structuration and anisotropic characteristics of the MRE material.

2. Materials and methods

2.1. Preparation of PDMS-Fe₃O₄@Ag MRE material

The preparation method used to obtain the textured composite with magnetic Fe₃O₄ silver-covered microparticles was described in detail in our previous articles [13, 14].

This procedure is briefly described here. First, Fe₃O₄ superparamagnetic nanoparticles (NPs) were synthesized by the chemical co-precipitation method, in which a solution mixture, (2:1) of FeCl₃·6H₂O and FeCl₂·4H₂O in chlorhydric acid, was added drop-by-drop to a solution of NaOH (60 °C, pH=14) under nitrogen atmosphere and high-speed stirring. The obtained nanocrystals were separated by repeated centrifugation and washing cycles, then dried in a vacuum oven at 40 °C for 24 h. The obtained dark brown NPs show a size distribution (determined by TEM images) with a maximum at 13 nm in the log-normal distribution of the diameters, which is in excellent agreement with the size of the crystallite domains calculated using the Debye-Scherrer relation from x-ray diffractograms (XRD), (14 ± 2) nm [20].

In the second step, the Fe₃O₄ NPs were covered with silver in order to obtain electrically conductive and superparamagnetic particles. For that, aqueous dispersions of Ag (NH₃)₂⁺ and Fe₃O₄ NPs in a 10:1 molar ratio were sonicated for 30 min at room temperature. Then, the system was heated in a water bath at 50 °C for 20 min with slow stirring. In the next step, 0.4 M glucose monohydrate solution was added drop-by-drop to the Fe₃O₄-Ag⁺ suspension. Stirring was continued for one hour. This synthesis protocol promotes the reduction of Ag (I) ions adsorbed onto Fe₃O₄ particles. The magnetite-silver particles were separated out from the solution by magnetization and then by centrifugation. After the particles were separated, the decanted supernatant liquid was fully transparent. The obtained system (referred to here as Fe₃O₄@Ag) is actually formed by microparticles whose internal structure consist of several Fe₃O₄ nanoparticles clusters covered by metallic silver, which is grouped together.

For the Fe₃O₄@Ag microparticles (MPs), the maximum diameter distribution is at 1.3 μm (determined by SEM and TEM images). For comparison purposes, silver particles (reddish orange) were produced in a separate batch using the same experimental conditions for each set.

Finally, a PDMS base and a curing agent, referred to as PDMS from now on (Sylgard 184, Dow Corning), were mixed in proportions of 10:1 (w/w) at room temperature and then loaded with the magnetic Fe₃O₄ silver-covered microparticles.

The chemistry that leads to the cross-linked polymer is summarized in scheme 1. Both of the commercial kit's components contain siloxane oligomers terminated with vinyl groups, **1**. The *curing agent* also includes cross-linking siloxane oligomers, **2**, which each contain at least three silicon-hydride bonds. The base includes a platinum-based catalyst that cures the elastomer by an organometallic cross-linking reaction [21, 22]. When **1**, **2** and the platinum-based catalyst (base and curing agent) are mixed together, the catalyst aids in the curing of the elastomer because it catalyzes

the addition of the Si-H bond (in **2**) across the vinyl groups (in **1**), forming Si-CH₂-CH₂-Si linkages (β -addition of a silicon hydrogen to the vinyl bond); this process is referred to as hydrosilation of the double bonds.

The multiple reaction sites on **2** allow for three-dimensional cross-linking. One advantage of this type of addition reaction is that no waste products are generated. In addition, changing the curing agent-to-base ratio alters the properties of the resulting cured elastomer; as the ratio of curing agent-to-base increases, a more rigid elastomer results. Increasing the temperature accelerates the cross-linking reaction [13, 24, 25].

The amounts of PDMS and fillers were weighed during mixing on an analytical balance, then they were homogenized and placed at room temperature in a vacuum oven for about two hours, until the complete absence of any air bubble. Specifically, composite material with 5% w/w of Fe₃O₄@Ag was prepared. The still fluid samples were incorporated into a specially designed cylindrical mold (1 cm diameter × 1.5 cm thickness) and placed between the magnetic poles of a Varian Low Impedance Electromagnet (model V3703), which provides highly homogeneous, steady magnetic fields. The mold was rotated at 30 rpm to preclude sedimentation and was heated at (75 ± 5) °C in the presence of a uniform magnetic field (**H**_{curing}, 0.35 T) for 3 h to obtain the cured material. Control samples, prepared without applying the magnetic field, were also obtained. More details are provided in references [13, 14, 16, 21, 26, 27]. Slices of the cured composites were held in an *ad-hoc* sample-holder and cut using a sharp scalpel; slices of 1.5 mm thickness (L) were obtained, which were used for the morphological (SEM analysis) and electrical characterization of the material as well, and for the manufacture of the stress sensor. The setup used to cut the slices provided slices of equal thickness (L = 1.5 mm) and similar areas (0.8 cm²) in both directions (parallel and perpendicular to the needles). Nevertheless, equal slices from the same sample, but with different thicknesses, were tested: L = 1.5 mm (used for preparing the sensors reported in the article) and L = 4 mm. The piezoresistive behavior of the samples with L = 4 mm thickness were very similar to that shown in figure 4(b) for samples with L = 1.5 mm thickness. The resistance (in ohms) is, of course, different, but very similar resistivities, (ρ , in ohms.cm) were obtained for both samples when compressed at a given stress.

Figure 1(a) shows a schematic representation of the PDMS-Fe₃O₄@Ag MRE fabrication process, while figure 2 shows, in detail, the internal structure of the designed material; the MRE is basically constituted by a polymer PDMS matrix with conductive pseudo-chains (needles), formed during curing of the polymer. The direction of the needles coincide with the direction of the magnetic field applied during the curing process. The conductive needles consist of agglomerations of Fe₃O₄@Ag microparticles, and the internal structure of each microparticle consists of several Fe₃O₄ nanoparticles clusters covered by metallic silver, which are grouped together (see figure 2). The separation between the clusters within a silver-covered microparticle was estimated to be about 10–15 nm [13].

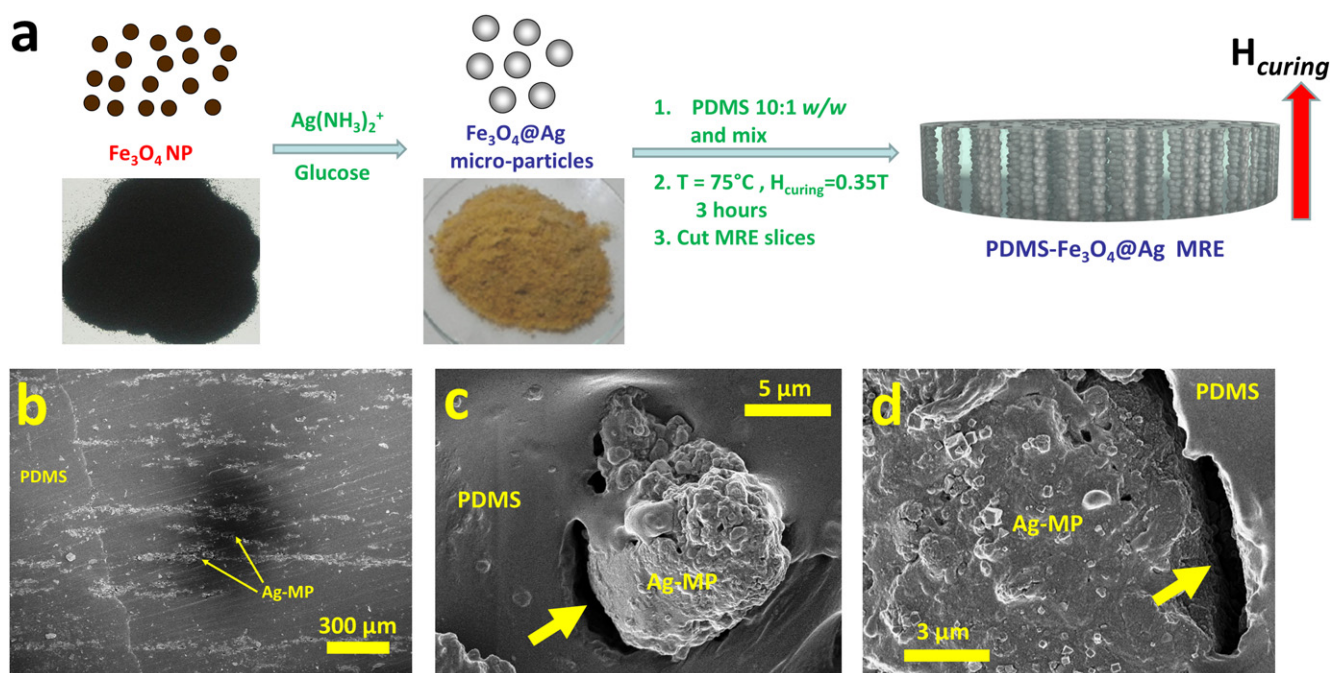


Figure 1. (a) Scheme of the MRE preparation process and photographs of Fe_3O_4 nanoparticles and $\text{Fe}_3\text{O}_4@\text{Ag}$ microparticles powders. SEM images of the structured PDMS- $\text{Fe}_3\text{O}_4@\text{Ag}$ MRE 5% w/w composite. (b) Lateral view showing the conductive needles. (c) Top view of one needle. (d) Magnified top view image. In (c) and (d), the arrows indicate the no-adhesion zone between the needles and the polymeric matrix (thickness ≈ 900 nm). 'Ag-MP' indicates the $\text{Fe}_3\text{O}_4@\text{Ag}$ microparticles filler, and 'PDMS' indicates the polymer matrix.

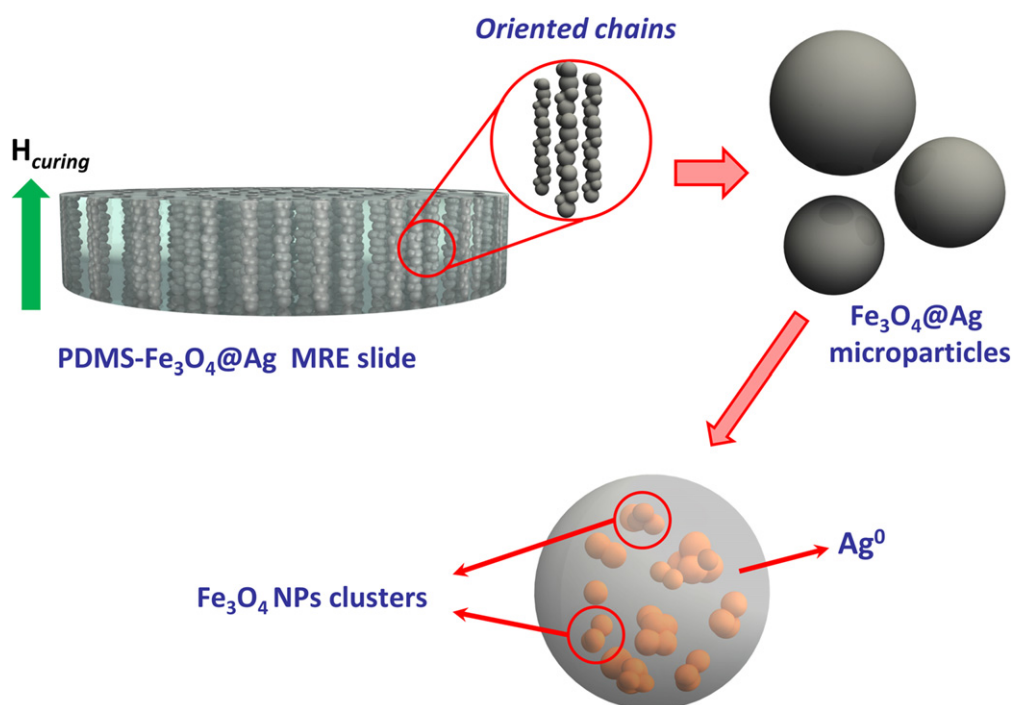


Figure 2. Internal structure of the designed material. The MRE is basically constituted by a PDMS matrix with conductive pseudo-chains (needles) that are formed when curing in the presence of a magnetic field, $\mathbf{H}_{\text{curing}}$. The needles are formed and aligned parallel to $\mathbf{H}_{\text{curing}}$. The conductive needles consist of agglomerations of $\text{Fe}_3\text{O}_4@\text{Ag}$ microparticles, and the internal structure of each microparticle consists of several Fe_3O_4 nanoparticle (NPs) clusters covered by metallic silver, which is grouped together.

The morphology of the PDMS- $\text{Fe}_3\text{O}_4@\text{Ag}$ composite was studied using a Field Emission Scanning Electron Microscope, FESEM (Zeiss Supra 40 Gemini). The composites were metalized for the purpose of obtaining the SEM

images. About 100 SEM images at several magnifications (from 50x to 6000x) were used to estimate the average dimensions of the needles. Voltages (EHT) of 5 KV and magnifications of 100x (3300 pixels/cm) and 300x (9800

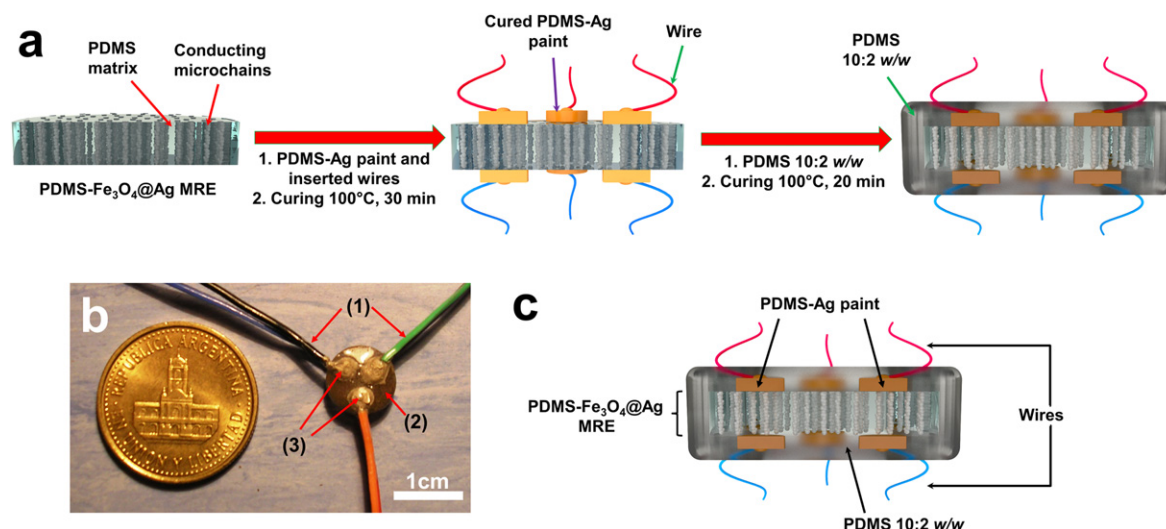


Figure 3. (a) Scheme summarizing the process of manufacturing the sensor. (b) Photograph of the sensor array next to an Argentinean $\text{¢}25$ coin: (1) wires, (2) sensing active material (PDMS-Fe₃O₄@Ag MRE) and (3) PDMS-Ag silver contacts. (c) Schematic diagram of the flexible stress array. Representations of longitudinal cuts of the sensor are shown in (a) and (c).

pixels/cm) were the typical conditions used for determining the average chain length, while 3 KV and 4000x (40 pixels/ μm) were used for obtaining the average chain diameter.

2.2. Implementation of the electrical contacts

In order to obtain metal contacts that are directly located on the surface of a slice of PDMS-Fe₃O₄@Ag MRE, a composite prepared by mixing conductive silver paint (SPI Conductive Silver Paint, SPI Supplies) and PDMS (base: cross-linker agent ratio = 10:2 w/w) was used, which is referred to as PDMS-Ag paint. The used conductive silver paint consists of a highly concentrated suspension, about $(43 \pm 3) \% \text{ w/w}$, of metallic silver powder dispersed in an acrylic resin-based organic that acts as a suspending and binder system. A small amount of PDMS (2% w/w) was added to the silver paint suspension (98% w/w of silver paint) to prepare the PDMS-Ag paint. Excellent electrical conductivity (resistivity lower than $3.2 \Omega \text{ cm}$) and excellent adhesion to the PDMS-Fe₃O₄@Ag MRE slice were obtained after curing in a vacuum oven at 100 °C for 30 min. The larger amount of the cross-linker agent (compared to that used in preparing the PDMS-Fe₃O₄@Ag MRE) allows for the obtainment of low elasticity contacts, thereby preventing its conductivity from varying significantly with the applied stress (ensuring that the change in conductivity of the sensor with the applied stress is only due, practically, to the effect of stress on the PDMS-Fe₃O₄@Ag MRE).

The PDMS-Ag paint, thus prepared, was used to place three pairs of contacts on the surface of the PDMS-Fe₃O₄@Ag MRE. The surface of the elastomer was previously cleaned with ethanol. The contacts were made carefully by first making the contacts on one side and then making them on the other. The fluid mixture PDMS-Ag paint was deposited on one side of the MRE surface using a syringe. Then, metallic wires were inserted into the PDMS-Ag Paint mixture while still fluid, followed by curing in an oven at

100 °C for 30 min under air ambient atmosphere. This procedure was then repeated when making the contacts on the other side of the MRE surface. The MRE PDMS-Fe₃O₄@Ag composite, at the used filler concentration, is highly transparent to visible light, which allows viewing of the positions in order to control the matching between opposed contacts. It also allows for the visual inspection of the contact's area during the process. All of the contacts of the PDMS-Fe₃O₄@Ag MRE slice top surface matches vertically with the contacts of the bottom surface, as illustrated in figure 3.

Additionally, PDMS-graphite and PDMS-multiwall carbon nanotube (MWCNT) composites were prepared with various percentages of filler (20–80% w/w) in order to test and compare their properties as an electrical contact. All these contact composites were discarded because of their low electrical conductivity and unwanted rheological and adherence properties; this is consistent with results obtained in other studies. [26, 28–30] For instance, the electrical resistivity of the composites made with these fillings (graphite and MWCNT) was very high compared to the material-sensitive MRE. Increasing the amount of filler increases the electrical conductivity, but it also increases its fragility (the contact material is easily fractured) and greatly reduces the adhesion of the contact composite to the MRE polymer material.

2.3. Packaging of the sensor's array

Finally, the composite and the contacts (sensor array) were covered with PDMS 10:2 w/w⁻¹ and again cured at 100 °C for 20 min. Electrical isolation of the whole measuring system (including contacts) is obtained with this coverage, which also provides resistance against chemical and physical agents. Figure 3(a) shows a scheme that summarizes the process of manufacturing the MRE-based stress sensor. Figure 3(b) shows a photograph of the sensor array next to an Argentinean $\text{¢}25$ coin. Figure 3(c) shows a schematic diagram of the flexible stress sensor array.

2.4. Elastic properties, piezoresistivity, magnetoresistance and sensor testing

A TEQ 4 (Argentina) potentiostat was used for the voltammetric and chronoamperometric measurements that were performed in order to evaluate the response of the elastomer composites to the applied voltage during on-off commutation cycles and to determine the current-voltage (I–V) characteristic curves of the different composites and of the sensor.

A specially designed device was used for measuring the piezoresistivity of the three concepts: 1) the PDMS-Fe₃O₄@Ag MRE, 2) the PMDS-Ag paint and 3) the sensor. The mentioned device includes two plastic plates that compress the samples and allow the application of the required force, along with a force sensor and a supporting metal structure. The compressive force was monitored by the force sensor. The voltammetric response was simultaneously recorded using the TQ4 potencioestat at different stresses.

The device for measuring magnetoresistance of the sensor consists of placing the setup described above between the pole pieces of an electromagnet that generates a uniform magnetic field. A Gaussmeter (Group3 DTM-133 Digital Teslameter) was used to test the intensity of the magnetic field. To measure the electrical resistivity in the MRE samples for different values of **H**, the current flux through the sample was measured under different intensities of **H**, while arbitrary and constant stress were applied.

Specific details of the elastic measurements were previously described [13, 14, 16, 27]. Samples for elasticity analysis were prepared by cutting the cured composites in the transversal and longitudinal directions with respect to the applied magnetic field during the curing process.

3. Results and discussion

The magnetic, electric, chemical and morphological properties of both Fe₃O₄ NPs and Fe₃O₄@Ag microparticle powders were characterized in a previous work by applying several techniques: VSM and SQUID (ZFC and FC curves) for magnetic; cyclic voltammetry for the electrical; XRD, UV-Vis, FTIR and EDS for the chemical; and XRD, and TEM and SEM for the morphological properties [12]. From those studies, it was assessed that the Fe₃O₄@Ag synthesized powder material had ohmic behavior, is in the superparamagnetic state for $T > 179$ K (blocking temperature at **H**=0), has a silver content of 82% *w/w*, exhibits proper oxygen stoichiometry (3:4 Fe-O) inverse spinel structure of the iron oxide core, and that all the Fe₃O₄ particles are covered with silver.

Therefore, in the next sections, only results concerning the properties of the MRE PDMS composites (including the contacts composite and MRE-based stress sensor), but not of the fillers, are presented and discussed.

3.1. PDMS composites

3.1.1. Morphology, magnetic and elastic properties of PDMS-Fe₃O₄@Ag MRE. The formation of macroscopic needles of

inorganic material, observable by the naked eye, was obtained using the protocol described in section 2.1. SEM images of the obtained slices are shown in figures 1(b), (c) and (d). The formation of needles was observed when Fe₃O₄@Ag was used as a filler, but only in the case of curing the PDMS in the presence of an applied field. In the absence of a magnetic field applied during curing an isotropic composite with Fe₃O₄@Ag microparticles homogeneously distributed in the PDMS matrix is obtained. The calculated average diameter, apparent length and areal density of the needles are 10.4 μ m, 1.35 mm and 8.4 needles mm⁻², respectively, which were obtained from analyzing the SEM images.

The observation of non-adhesion zones between the matrix and the filler (shown in figure 1) seems not to be induced by the slice preparation (e.g., the manner of cutting the slices) but as a consequence of the relatively low degree of interaction between the polydimethylsiloxane chains and the filler particles in the cured material. For instance, Van der Waals interactions between PDMS and the metallic needles (pseudo-chains) are very low and, since the filler particles were not derivatized, there are no covalent unions either. The hypothesis that the non-adhesion zones are originated by the absence of strong PDMS-needle interaction is supported not only because of the lack of correlations with manners of cutting but also by the absence of any appreciable change in the physical properties of the slices after the first compression or extension. This effect, referred to as the Mullin effect [31–34], was never observed in the presented composite materials. The lack of observation of a significant elastic hysteresis is interpretable as the absence of an appreciable Mullins effect. This behavior was observed regardless of the direction of compression (\parallel or \perp in respect to the needles) probably because of the separation (non-adhesion) between the polymer matrix and needles. In figures 1(c) and (d), the arrow indicates the no-adhesion zone between the inorganic filler and the polymeric matrix (thickness \approx 900 nm) in a SEM top view of a chain.

Concerning the magnetic behavior of the MRE composite, the system presents superparamagnetic behavior at room temperature. The superparamagnetic behavior at room temperature provides a relatively fast magnetic relaxation (loss of magnetization after canceling the applied external magnetic field), which, in the present composites, occurred faster than the time resolution of our setup (3 s). The superparamagnetic behavior is lost for temperatures below the blocking temperature, T_B . Values of $T_B = 175$ K and $T_B = 168$ K at **H**=0.01 T were obtained from the ZFC-FC magnetization *vs* temperature curves in the directions parallel and perpendicular to the needles, respectively. Results are similar to those described previously [13].

It is important to remark that the superparamagnetic behaviour at 298 K is conserved in the Fe₃O₄@Ag microparticles (and thus, in the Fe₃O₄@Ag-PDMS composite) when the Fe₃O₄ nanoparticles are in the superparamagnetic state. This indicates that the size of the Fe₃O₄ nanoparticles (13 nm) is small enough to prevent cooperative effects that could (eventually) induce a ferrimagnetic order due to interactions that occur even inside the Fe₃O₄@Ag

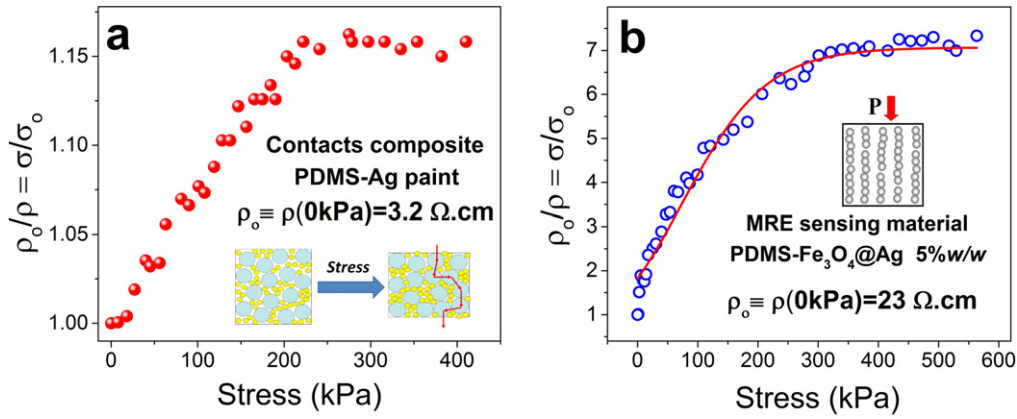


Figure 4. (a) Relative resistivity of PDMS-Ag paint (contacts) as a function of \mathbf{P} . (b) Relative resistivity of PDMS-Fe₃O₄@Ag MRE material (5% w/w filler concentration) as a function of \mathbf{P} . The solid line represents the model fit (equation (3) in [13] with $\mathbf{H}=0$). The transverse resistivity maintained a value of 62 M Ω cm, regardless of the stress.

agglomerate. In other words, the interactions between the particles cannot effectively compete with the thermal disorder in order to establish a magnetic order at 298 K (blocking temperature is much lower, $T_B \cong 170$ K) when the average size of the individual particles that constitute the agglomerate is below some critical value.

3.1.2. Piezoresistivity of PDMS-Fe₃O₄@Ag MRE material. In order to evaluate the piezoresistivity of PDMS-Fe₃O₄@Ag MRE, electrical conductivities (in $\Omega^{-1} \text{cm}^{-1}$) were obtained parallel (σ_{\parallel}) and perpendicular (σ_{\perp}) to the direction of the needles as a function of the applied stress (\mathbf{P} , expressed in kPa). In all cases, the stress was applied in the same direction in which the electrical conductivity was measured. The variation of σ_{\parallel} with \mathbf{P} is shown in figure 4(b). On the other hand, $\sigma_{\perp} = 1.6 \cdot 10^{-8} \Omega^{-1} \text{cm}^{-1}$ was obtained independently of the applied stress ($\rho_{\perp} = 1/\sigma_{\perp} = 62 \text{ M}\Omega \text{cm}$). These results show that anisotropic conduction was obtained with significant conductivity only in the direction of the needles ($\rho_{\perp}/\rho_{\parallel}$) $\sim 10^6$. Electrical conductivity in the parallel direction increases with increasing stress in the range of 0–350 kPa. Experimental data were well fitted as a function of \mathbf{P} by a simple model described in our previous work [13], which assumes that the barrier for electrical conductance involved in electron-jumps decreases with \mathbf{P} . The solid line in figure 4(b) corresponds to that model (see equation (3) in ref. [13]).

3.1.3. Piezoresistivity of PDMS-Ag paint contacts. For the electric characterization of the PDMS-Ag paint composite used for contacts that adhered to the surface of the (PDMS-Fe₃O₄@Ag) MRE, the fluid mixture was placed in a rectangular mold 1 cm² area and 12 mm high and then cured under the established conditions (100 °C, 30 min), yielding a solid pellet of said composite. The obtained pellets were placed in the setup used to measure piezoresistivity (described in section 2.4). Figure 4(a) shows ρ_0/ρ vs \mathbf{P} , where ρ_0 is the resistivity of the PDMS-Ag paint composite at $\mathbf{P}=0$ kPa ($\rho_0 = 3.2 \Omega \text{cm}$). The shape of the curve corresponds to the well-known behavior of isotropic conducting particles-

polymer composites systems under strain induced by external mechanical stress, in which the percolation probability between neighboring particles must depart from a scale-invariant behavior but saturate at moderated-high strains, reaching the percolation path's saturation with sigmoid dependence. This dependence was already predicted in previously developed models [26, 35, 36], which propose a dynamic picture where contacts or bonds between neighboring particles are created but also destroyed when stress is applied in the composite.

Importantly, the conductivity of this material reaches its maximum value for $\mathbf{P} \sim 200$ kPa with only a 16% change in resistivity, $\Delta\rho$, defined as $\Delta\rho \equiv 100 \times (\rho_0 - \rho(\mathbf{P} = \infty))/\rho(\mathbf{P} = \infty)$ (much lower than what was observed for the PDMS-Fe₃O₄@Ag MRE when used as a sensor material, for which $\Delta\rho = 635\%$). This is a sought property (see section 2.2), which seems related to the low elasticity of the contacts in comparison with the MRE. In order to test this hypothesis, two different contacts varying the base/cross-linker ratio were implemented. The ratios used were 10:2 and 10:1 (w/w ratio base:cross-linker). The contacts obtained when using the higher ratio (10:2) display lower elasticity (deformation by compression requires more stress) and present a lower relative change in electrical resistivity, $\Delta\rho$. It was obtained by $\Delta\rho$ (10:2) = 16% while $\Delta\rho$ (10:1) = 48%. These results seem to indicate that a relative small change in the conductivity of the contacts (prepared using a (10:2) ratio) with the applied stress is related to its low elasticity.

3.2. Sensor: response and quality parameters

The performance of the packaged sensor array (encapsulated MRE material with contacts) is presented in this section. Cyclic voltammograms at different stresses and at room temperature are shown in figure 5(a) (scan rate 5 mV s⁻¹). The arrow shows the increase of the applied stress. These characteristic I-V curves show that the sensor presents ohmic behavior in the whole stress range (threshold or rectifier effects were not observed in that range).

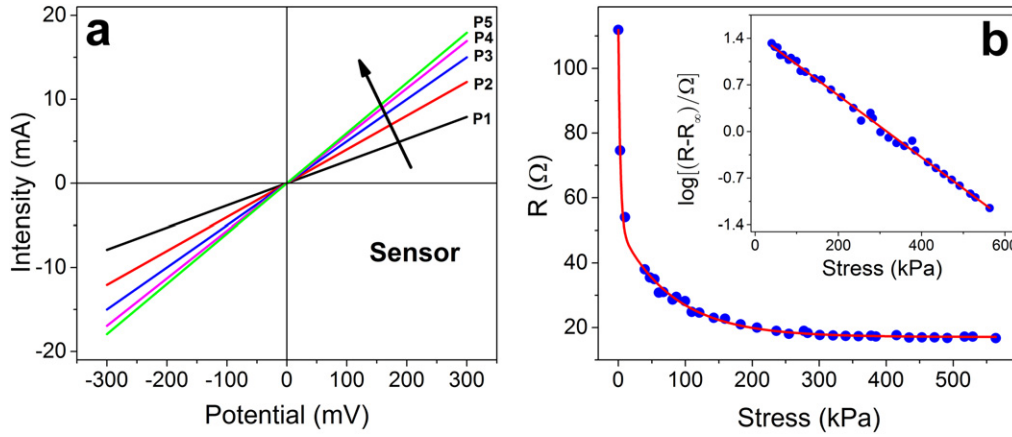


Figure 5. (a) Cyclic voltammograms under different applied stresses at room temperature. Scan rate: 5 mV s^{-1} . The arrow shows the increase of P : $P1 = 40 \text{ kPa}$; $P2 = 110 \text{ kPa}$; $P3 = 207 \text{ kPa}$; $P4 = 301 \text{ kPa}$; $P5 = 563 \text{ kPa}$. (b) The sensors' response expressed as resistance, R , versus P . The solid line represents the model fit given by equation (2). Inset: $\log[(R - R_\infty)/\Omega]$ versus P for $P > 40 \text{ kPa}$. The solid line represents the model fit by equation (1). The slope is $(5.43 \pm 0.02) \cdot 10^{-3} \text{ kPa}^{-1}$; the intercept is 1.53 ± 0.01 and $R^2 = 0.99947$.

Figure 5(b) shows the sensor's response under stress in terms of electrical resistance, R , vs P for one particular sensor of the array. The different array sensors have very similar responses to applied stress. It is noteworthy that the response curves of both sensor assemblies were unaffected after 3000 bending deformations, which shows the great strength of the material to such mechanical deformation. It is worth noting also that each sensor provides a response that is independent of the other array sensors. This enables mapping of the stress in a relatively extended area, although an array with a larger number of sensors should be used for that purpose.

It should be noted that conductivity curves, as a function of the applied stress, are not modified after 100 compressing-decompressing cycles, which constitutes a significant improvement over sensors based on MRE materials developed by other authors [37, 38]. Analogous to what happens with the elastic properties of the material, this can be justified in part by the absence of the Mullins effect [31, 32, 34]. In addition, conductivity curves as a function of the applied stress remained unchanged for at least ten months. This is a direct consequence of the chemical inertia of the filler against oxidation in the air, which also constitutes a significant improvement over the materials described so far [19, 39–43].

The dynamic range of all the sensors is between 0–350 kPa. Saturation of the response is obtained above 350 kPa. The piezoresistive response for any array sensor can be calibrated in the range of 0–350 kPa by a bi-exponential fit according to equation (1):

$$R(P) = R_\infty + A_1 \exp\left(-\frac{P}{\xi_1}\right) + A_2 \exp\left(-\frac{P}{\xi_2}\right) \quad \text{for } 0 \text{ kPa} \leq P \leq 350 \text{ kPa} \quad (1)$$

for $0 \text{ kPa} \leq P \leq 350 \text{ kPa}$ where $R_\infty = R(P = \infty)$ represents the measured electrical resistance at $P \gg 350 \text{ kPa}$. Excellent fits were obtained from the experimental result using equation (1) (see figure 5(b)). The solid line in figure 5(b) corresponds to the fits using equation (1) for the response of one particular

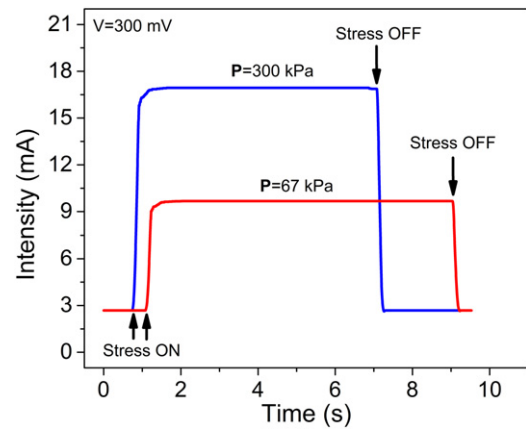


Figure 6. Current-time responses (sensorgrams) for one sensor of the array under two applied stresses. The applied voltage, V , is fixed to 300 mV.

sensor of the array. The recovered fitting parameters for the particular sensor are the following: $R_\infty = (17.1 \pm 0.2) \Omega$, $A_1 = (34 \pm 1) \Omega$, $\xi_1 = (81 \pm 3)$, $A_2 = (61 \pm 2) \Omega$ and $\xi_2 = (2.9 \pm 0.1) \text{ kPa}$ with $R^2 = 0.9982$.

A single exponential fit can be used for calibrations in the range of 40–350 kPa:

$$R(P) = R_\infty + A \exp\left(-\frac{P}{\xi}\right) \quad \text{for } 40 \text{ kPa} \leq P \leq 350 \text{ kPa} \quad (2)$$

In the case of the sensor considered in figure 5(b), the recovered parameters for the range 40–350 kPa are: $R_\infty = (17.1 \pm 0.2) \Omega$, $A = (34 \pm 1) \Omega$ and $\xi = (80 \pm 4) \text{ kPa}$ with $R^2 = 0.9960$. The inset of figure 5(b) shows the logarithmic response in the 40–350 kPa range. A linear calibration plot is obtained when representing $\log[(R - R_\infty)/\Omega]$ vs P and recovering a slope $S = (5.43 \pm 0.02) \cdot 10^{-3} \text{ decade kPa}^{-1}$, which provides the sensitivity of the system in the case of the described sensor.

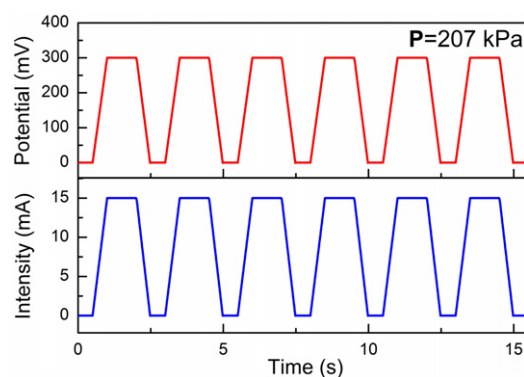


Figure 7. Commutation cycles for one sensor of the array. No electrical hysteresis was detected in the commutation cycles, and no phase delays between the detected current and applied voltage was observed within our time resolution scale (about 50 ms).

Figure 6 shows electrical current (I) versus time (t) responses (at a fixed voltage) for one sensor of the array under two different stresses. These I - t curves are the sensorgrams associated with the specific sensor. Larger applied stresses result in greater current. This finding is consistent with the piezoresistivity behavior described in the previous section: to increase the applied stress on the sensor produces a decrease of the resistance.

The relaxation and response times are also evaluated. The relaxation time (τ_{relax}) is defined as the time it takes to recover the base current after releasing the stress, while the response time (τ_{resp}) is the time it takes to reach the signal (current intensity) associated with a given stimulus (stress). The relaxation times ($\tau_{\text{relax}}(300 \text{ kPa}) = 450 \text{ ms}$ and $\tau_{\text{relax}}(67 \text{ kPa}) = 220 \text{ ms}$) are smaller than the response times ($\tau_{\text{resp}}(300 \text{ kPa}) = 935 \text{ ms}$ and $\tau_{\text{resp}}(67 \text{ kPa}) = 1100 \text{ ms}$). In particular, the relaxation time of any sensor in the array is very similar to the relaxation time of the PDMS- Fe_3O_4 @Ag MRE in the elastic relaxation curves [13, 14]. This result demonstrates that the presence of the contacts and the cover of PDMS do not significantly affect the relaxation of the stress's sensitive material.

Figure 7 shows commutation cycles for one sensor of the array. No electrical hysteresis was detected in the commutation cycles, and no phase delays between the detected current and applied voltage was observed within our time resolution scale (about 50 ms).

To evaluate the change of sensor response with the temperature, the electrical resistance for each of the array sensors was measured as a function of temperature under an arbitrary fixed stress. The I - V characteristic curves were measured by placing the array in an oven at different temperatures in the range of 25–155 °C and applying a stress of 54 kPa. The results are shown in figure 8, and clearly demonstrate that the temperature does not significantly modify the response of the sensor, since the electrical resistance increases by only 6.3% percent from 25 °C to 155 °C. This change is much lower than those previously reported for other metallic filler based-MRE materials [37, 44–46]. The obtained value of the thermal resistive coefficient is $\alpha = (1/R)$

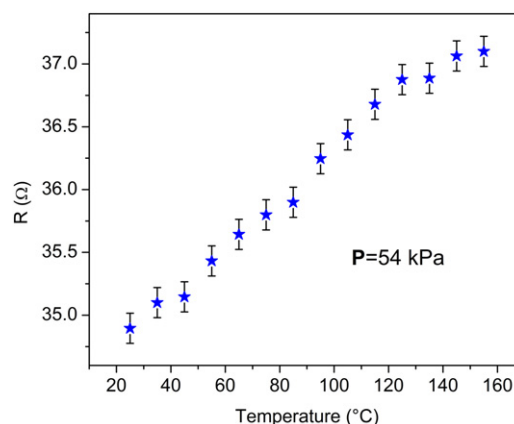


Figure 8. Change in sensor response with temperatures in the range of 25–155 °C at a fixed stress ($P = 54 \text{ kPa}$). The variation in the whole range of temperatures is less than 6%.

$\times (\partial R / \partial T) = 5.0 \times 10^{-4} \text{ K}^{-1}$. This value, although relatively very low, is positive and therefore in agreement with a decrease of percolation probability between needles with thermal expansion. The small observed dependence to temperatures up to 155 °C can be interpreted by observing that: a) the system is still far from the glass transition temperature (T_g) of PDMS Sylgard 184 1:10 w/w^{-1} ($T_g \approx 450 \text{ °C}$) [47], where changes with temperature are expected to be larger; b) the value of the thermal expansion coefficient of the polymer matrix is relatively small (compared to those of matrixes used in [44–46], for instance). These factors predict little change in the average distance between conductive needles with temperatures in the considered range, and hence, predict little modification in the piezoresistive response of the sensor, as observed.

Finally, it is of great interest to evaluate whether the sensor is degraded by chemical agents. Therefore, the sensor array was immersed in various organic solvents (ethanol, methanol, isopropanol, dichloromethane, chloroform, acetone, acetonitrile, benzene and toluene, Sigma Aldrich), along with water and a NaCl aqueous saturated solution for 48 h. Then, the array was washed and assessed for damages in the material. Treatment of the sensor array in these media did not cause wear; a visual inspection showed no damage to the surface of the material, and the response curves of the immersed sensors do not show any noticeable differences from the curve shown in figure 5(b).

In addition to the magnetic properties described in section 3.1.1, the synthesized hybrid polymer material has negative magnetoresistance [13]. This property is inherited by the developed sensor. Indeed, figure SM1 (see supplementary material, available at stacks.iop.org/SMS/23/085026/mmedia) shows the variation of the electrical resistance of any array sensor by application of a magnetic field at constant arbitrary stress ($P = 100 \text{ kPa}$). The electrical resistance decreases monotonically with the applied magnetic field (negative magnetoresistance). These properties suggest that the sensor described in this work can be potentially used as a magnetic field sensor also (under a fixed stress).

4. Conclusions

The technological challenges mentioned in the Introduction were satisfactorily resolved by the use of polymeric composites: a) the active sensing material is a structured elastomer composite (the MRE material); b) the contacts are made of a PDMS-Ag paint composite; c) the final packaging is made of cured PDMS. The silver-covered inorganic material–polymer composite, PDMS-Fe₃O₄@Ag, is the sensing element, which displays elastic, magnetic and electrical anisotropic and reversible properties. Using this material, a flexible and portable stress sensor prototype was designed, manufactured and characterized. The array device consists of three parts: i) a slice of the sensing MRE material (PDMS-Fe₃O₄@Ag 5% w/w), ii) the metallic-like contact based on PDMS and an Ag-paint (acrylic resin with metallic silver powder mixture) located directly on the surface of the MRE material, and iii) the PDMS insulator layer.

The dynamic range of the sensors is 0–350 kPa. A bi-exponential fit can be used to calibrate the response in that whole range, although a single exponential relationship fits well between 40–350 kPa. The responses of the sensors are fully reversible with stress, which is one of the main goals of the developed system. These conclusions are valid for any array sensor.

The number of sensors per unit area of sensing element (Fe₃O₄@Ag-PDMS) can be increased greatly. Furthermore, the sensing MRE material allows for the changing of different variables, such as the magnetic field during curing (H_{curing}) and the filler concentration in the range of 5–10% w/w. These variables can be optimized for the particular desired application, such as Zebra®-like 2D connectors (connectors for parallel flip-chip connections with elastic behavior, which display anisotropic piezoresistivity that can be used to modulate the conduction between contact points) or flexible stress sensors. A key issue for these applications is the highly reproducible electrical response of the prepared composites after successive cycles of applied external stress.

Transversal conduction was not observed for any sensor of the array system; thus, the composite essentially behaves as an insulator in that direction. On the other hand, the longitudinal electrical conduction (parallel to the needles) presents ohmic behavior though the whole range of stress. That is, the sensor is anisotropic; it senses changes when stress is exerted parallel to the direction of the needles created exclusively in the MRE material. This is an interesting property for many applications, such as those mentioned below.

No electrical hysteresis was detected in the commutation cycles, and no phase delays between the detected current and applied voltage were observed within our time resolution scale (about 50 ms). All these properties give particular importance to the developed sensor for the development of extended stress mapping such as artificial skins.

The properties described here make the present system an interesting alternative to a stress sensor array in aggressive environments where traditional sensors with high metal content or semiconductor behavior cannot be used. The sensor described in this paper could also be used in force

measurement in hard-to-access places, such as in geological exploration for the purpose of weighing rocky material in soil borings. In the field of biometrics, it could be used for heart rate measurements (beats per minute), since it has a fast response time. It is lightweight, portable and non-invasive, which makes it appropriate to measure a pulse in real time during 24 h. In the latter case, it is necessary to optimize the detection limit of the device. This can be performed by modifying the synthetic variables, such as the amount of filler used in the manufacture of the MRE, its magnetization, the magnetic field intensity applied during curing, the polymer matrix, etc.

The array is not altered or damaged by exposition to common organic solvents (aliphatic, aromatic and chlorinated), water or salt solutions. Ambient air oxidation was not observed. These properties make the present system an interesting alternative to a stress sensor array in aggressive environments where traditional sensors with high metal content or semiconductor behavior cannot be used.

Acknowledgments

GJ and RMN are research members of the National Council of Research and Technology (CONICET, Argentina). JLM is a PhD student at the University of Buenos Aires (UBA). Financial support was received from the UBA (UBACyT 2012-2015, project 2002 01101 00098), and the Ministry of Science, Technology and Innovations (MINCYT-FONCYT, Argentina, PICT 2011-0377). The authors thank the *Laboratorio de Bajas Temperaturas* (School of Sciences, UBA) for facilities concerning magnetic measurements and preparation of the structured MRE materials. Dr Pablo I Tamborenea (UBA) is acknowledged for contributing useful discussions, and Industrial Designer Luciana Feo Mourelle is acknowledged for designing the images representing the MRE. The Center of Documental Production (CePro) and the Center of Advanced Microscopy (CMA), School of Sciences, University of Buenos Aires, are acknowledged for obtaining the presented pictures and SEM-TEM images.

References

- [1] Li W H, Zhang X Z and Du H 2013 Magnetorheological elastomers and their applications *Advances in Elastomers I: Advanced Structured Materials* ed P M Visakh, S Thomas, A K Chandra and A P Mathew (Berlin: Springer) pp 357–74
- [2] Danas K, Kankanala S V and Triantafyllidis N 2012 Experiments and modeling of iron-particle-filled magnetorheological elastomers *J. Mech. Phys. Solids* **60** 120–38
- [3] Bica I, Liu Y D and Choi H J 2012 Magnetic field intensity effect on plane electric capacitor characteristics and viscoelasticity of magnetorheological elastomer *Colloid Polym. Sci.* **290** 1115–22
- [4] Varga Z, Filipcsei G and Zrínyi M 2006 Magnetic field sensitive functional elastomers with tuneable elastic modulus *Polymer* **47** 227–33

- [5] Ivaneyko D, Toshchevikov V P, Saphiannikova M and Heinrich G 2011 Magneto-sensitive elastomers in a homogeneous magnetic field: a regular rectangular lattice model *Macromol. Theory Simul.* **20** 411–24
- [6] Shahriyar K and Vicente J de 2013 Thermoresponsive polymer-based magneto-rheological (MR) composites as a bridge between MR fluids and MR elastomers *Soft Matter* **9** 11451–6
- [7] Stepanov G V, Abramchuk S S, Grishin D A, Nikitin L V, Kramarenko E Y and Khokhlov A R 2007 Effect of a homogeneous magnetic field on the viscoelastic behavior of magnetic elastomers *Polymer* **48** 488–95
- [8] Varga Z, Filipcsei G and Zrínyi M 2006 Magnetic field sensitive functional elastomers with tuneable elastic modulus *Polymer* **47** 227–33
- [9] Keshoju K and Sun L 2009 Mechanical characterization of magnetic nanowire-polydimethylsiloxane composites *J. Appl. Phys.* **105** 023515
- [10] Yang I-H, Yoon J-H, Jeong J-E, Jeong U-C, Kim J-S, Chung K H and Oh J-E 2013 Magnetic-field-dependent shear modulus of a magnetorheological elastomer based on natural rubber *J. Korean Phys. Soc.* **62** 220–8
- [11] Kchit N and Bossis G 2008 Piezoresistivity of magnetorheological elastomers *J. Phys.: Condens. Matter.* **20** 204136
- [12] Koo J-H, Khan F, Jang D-D and Jung H-J 2010 Dynamic characterization and modeling of magneto-rheological elastomers under compressive loadings *Smart Mater. Struct.* **19** 117002
- [13] Mietta J L, Ruiz M M, Antonel P S, Perez O E, Butera A, Jorge G and Negri R M 2012 Anisotropic magnetoresistance and piezoresistivity in structured Fe₃O₄-silver particles in PDMS elastomers at room temperature *Langmuir* **28** 6985–96
- [14] Mietta J L, Jorge G, Perez O E, Maeder T and Negri R M 2013 Superparamagnetic anisotropic elastomer connectors exhibiting reversible magneto-piezoresistivity *Sensors Actuators A* **192** 34–41
- [15] Denver H, Heiman T, Martin E, Gupta A and Borca-Tasciuc D-A 2009 Fabrication of polydimethylsiloxane composites with nickel nanoparticle and nanowire fillers and study of their mechanical and magnetic properties *J. Appl. Phys.* **106** 064909
- [16] Landa R A, Antonel P S, Ruiz M M, Perez O E, Butera A, Jorge G, Oliveira C L P and Negri R M 2013 Magnetic and elastic anisotropy in magnetorheological elastomers using nickel-based nanoparticles and nanochains *J. Appl. Phys.* **114** 213912
- [17] Yang J, Gong X, Zong L, Peng C and Xuan S 2013 Silicon carbide-strengthened magnetorheological elastomer: Preparation and mechanical property *Polym. Eng. Sci.* **53** 2615–23
- [18] Bica I, Anitas E M, Bunoiu M, Vatzulik B and Juganaru I 2014 Hybrid magnetorheological elastomer: influence of magnetic field and compression pressure on its electrical conductivity *J. Ind. Eng. Chem.* (doi:10.1016/j.jiec.2013.12.102)
- [19] Stoll A, Mayer M, Monkman G J and Shamonin M 2014 Evaluation of highly compliant magneto-active elastomers with colossal magnetorheological response *J. Appl. Polym. Sci.* **131** 39793
- [20] Godoy M, Moreno A J, Jorge G A, Ferrari H J, Antonel P S, Mietta J L, Ruiz M, Negri R M, Pettinari M J and Bekeris V 2012 Micrometric periodic assembly of magnetotactic bacteria and magnetic nanoparticles using audio tapes *J. Appl. Phys.* **111** 044905
- [21] Butera A, Álvarez N, Jorge G, Ruiz M M, Mietta J L and Negri R M 2012 Microwave response of anisotropic magnetorheological elastomers: Model and experiments *Phys. Rev. B* **86** 144424
- [22] Auner N and Weis J 2008 *Organosilicon Chemistry III: From Molecules to Materials* (New York: Wiley)
- [23] Efimenko K, Wallace W E and Genzer J 2002 Surface modification of Sylgard-184 poly(dimethyl siloxane) networks by ultraviolet and ultraviolet/ozone treatment *J. Colloid Interface Sci.* **254** 306–15
- [24] Eita M, El Sayed R and Muhammed M 2012 Optical properties of thin films of zinc oxide quantum dots and polydimethylsiloxane: UV-blocking and the effect of cross-linking *J. Colloid Interface Sci.* **387** 135–40
- [25] Esteves A C C, Brokken-Zijp J, Laven J, Huinink H P, Reuvers N J W, Van M P and de With G 2009 Influence of cross-linker concentration on the cross-linking of PDMS and the network structures formed *Polymer* **50** 3955–66
- [26] Negri R M, Rodríguez S D, Bernik D L, Molina F V, Pilosof A and Perez O 2010 A model for the dependence of the electrical conductance with the applied stress in insulating-conducting composites *J. Appl. Phys.* **107** 113703
- [27] Ruiz M M, Mietta J L, Soledad Antonel P, Pérez O E, Martín Negri R and Jorge G 2013 Structural and magnetic properties of Fe_{2-x}CoSm_xO₄—nanoparticles and Fe_{2-x}CoSm_xO₄—PDMS magnetoelastomers as a function of Sm content *J. Magn. Magn. Mater.* **327** 11–9
- [28] Liu C-X and Choi J-W 2010 Strain-dependent resistance of PDMS and carbon nanotubes composite microstructures *IEEE Trans. Nanotechnol.* **9** 590–5
- [29] Shih W-P, Tsao L-C, Lee C-W, Cheng M-Y, Chang C, Yang Y-J and Fan K-C 2010 Flexible temperature sensor array based on a graphite-polydimethylsiloxane composite *Sensors* **10** 3597–610
- [30] Lu J, Lu M, Bermak A and Lee Y-K 2007 Study of piezoresistance effect of carbon nanotube-PDMS composite materials for nanosensors *7th IEEE Conf. on Nanotechnology (2007)* pp 1240–3
- [31] Coquelle E, Bossis G, Szabo D and Giulieri F 2006 Micromechanical analysis of an elastomer filled with particles organized in chain-like structure *J. Mater. Sci.* **41** 5941–53
- [32] Coquelle E and Bossis G 2006 Mullins effect in elastomers filled with particles aligned by a magnetic field *Int. J. Solids Struct.* **43** 7659–72
- [33] Schmoller K M and Bausch A R 2013 Similar nonlinear mechanical responses in hard and soft materials *Nat. Mater.* **12** 278–81
- [34] Diani J, Fayolle B and Gilormini P 2009 A review on the Mullins effect *Eur. Polym. J.* **45** 601–12
- [35] Sreeprasad T S, Rodriguez A A, Colston J, Graham A, Shishkin E, Pallem V and Berry V 2013 Electron-tunneling modulation in percolating network of graphene quantum dots: fabrication, phenomenological understanding, and humidity/pressure sensing applications *Nano Lett.* **13** 1757–63
- [36] Shehzad K, Zha J-W, Zhang Z-F, Yuan J-K and Dang Z-M 2013 Piezoresistive behavior of electrically conductive carbon fillers/thermoplastic elastomer nanocomposites *J. Adv. Phys.* **2** 70–4
- [37] Kchit N and Bossis G 2009 Electrical resistivity mechanism in magnetorheological elastomer *J. Phys. D: Appl. Phys.* **42** 105505
- [38] Zavickis J, Knite M, Podins G, Linarts A and Orlovs R 2011 Polyisoprene-nanostructured carbon composite—a soft alternative for pressure sensor application *Sensors Actuators A* **171** 38–42
- [39] Bica I, Liu Y D and Choi H J 2013 Physical characteristics of magnetorheological suspensions and their applications *J. Ind. Eng. Chem.* **19** 394–406
- [40] Bica I, Liu Y D and Choi H J 2012 Magnetic field intensity effect on plane electric capacitor characteristics and viscoelasticity of magnetorheological elastomer *Colloid Polym. Sci.* **290** 1115–22

- [41] Yu M, Ju B, Fu J, Liu X and Yang Q 2012 Influence of composition of carbonyl iron particles on dynamic mechanical properties of magnetorheological elastomers *J. Magn. Magn. Mater.* **324** 2147–52
- [42] Dong X, Ma N, Ou J and Qi M 2013 Predicating magnetorheological effect of magnetorheological elastomers under normal pressure *J. Phys.: Conf. Ser.* **412** 012035
- [43] Qiao X, Lu X, Li W, Chen J, Gong X, Yang T, Li W, Sun K and Chen X 2012 Microstructure and magnetorheological properties of the thermoplastic magnetorheological elastomer composites containing modified carbonyl iron particles and poly(styrene-*b*-ethylene-ethylenepropylene-*b*-styrene) matrix *Smart Mater. Struct.* **21** 115028
- [44] Lundberg B and Sundqvist B 1986 Resistivity of a composite conducting polymer as a function of temperature, pressure, and environment: applications as a pressure and gas concentration transducer *J. Appl. Phys.* **60** 1074–9
- [45] Martin J E, Anderson R A, Odinek J, Adolf D and Williamson J 2003 Controlling percolation in field-structured particle composites: observations of giant thermoresistance, piezoresistance, and chemiresistance *Phys. Rev. B* **67** 094207
- [46] Kchit N, Lancon P and Bossis G 2009 Thermoresistance and giant magnetoresistance of magnetorheological elastomers *J. Phys. D: Appl. Phys.* **42** 105506
- [47] Lv P, Wang Z, Hu Y and Yu M 2009 Study on effect of polydimethylsiloxane in intumescent flame retardant polypropylene *J. Polym. Res.* **16** 81–9